

Numerical Modelling of Scramjet Combustor

M. Deepu¹, S.S. Gokhale², and S. Jayaraj³

¹*N.S.S. College of Engineering, Palakkad, Kerala-678 008*

²*Indian Institute of Technology Madras, Chennai-600 036*

³*National Institute of Technology, Calicut, Kerala-673 601*

ABSTRACT

Numerical modelling of turbulent-reacting flow field of supersonic combustion ramjet (scramjet) combustors are presented. The developed numerical procedure is based on the implicit treatment of chemical source terms by preconditioning and solved along with unsteady turbulent Navier-Stokes equations explicitly. Reaction is modelled using an eight-step hydrogen-air chemistry. Code is validated against a standard wall jet experimental data and is successfully used to model the turbulent-reacting flow field resulting due to the combustion of hydrogen injected from diamond-shaped strut and also in the wake region of wedge-shaped strut placed in the heated supersonic airstream. The analysis could demonstrate the effect of interaction of oblique shock wave with a supersonic stream of hydrogen in its (fuel-air) mixing and reaction for strut-based scramjet combustors.

Keywords: Scramjet, strut injector, supersonic combustor, reduced chemistry, point implicit method, FVM

NOMENCLATURE

c	Sound velocity	k_b	Backward reaction rate
C	Chemical species	K	Thermal conductivity
C_v	Specific heat at constant volume	p	Pressure
C_p	Specific heat at constant pressure	Q	Heat flux
D'	Effective exchange coefficient	S	Chemical source term
E	Total energy	U	Vector of conservation variables
F & G	Flux vectors	u	Velocity in x -direction
f	Stoichiometric hydrogen-air mass ratio	v	Velocity in y -direction
κ	Kinetic energy of turbulence	γ	Molecularity of a reaction
k_f	Forward reaction rate	ρ	Density
		ε	Kinetic energy dissipation

τ	Shear stress
μ	Viscosity
Γ	Surface area
Ω	Cell volume
∇^2	Laplacian operator
Δt	Time step

Subscripts

i	Chemical species
j	Reaction steps
l	Laminar
t	Turbulent

Superscripts

'	Reactant
"	Product

1. INTRODUCTION

Supersonic combustion ramjet (scramjet) combustor benefits from the better performance of an air-breathing propulsion system. Scramjet needs a combustor having an efficient (fuel-air) mixing and combustion of fuel with air at supersonic speeds without much pressure loss^{1,2}. Many experimental and numerical analyses have been reported during the last few decades wrt the characteristics of the complex flow field, resulting due to fuel-air mixing and combustion. Strut-based parallel fuel injectors are preferred in combustors of air-breathing propulsion systems, as the overall pressure loss associated with it is minimum when compared to the normal injection. Riggins^{3,4}, *et al.* have shown that incomplete mixing, shock waves, and viscous effects are the main factors leading to the thrust loss in supersonic combustors, though these effects aid mixing. Strut injectors offer a possibility for parallel injection without causing much blockage to the incoming stream of air, and also the fuel can be injected at the core of the stream. Tomioka^{5,6}, *et al.* studied the effects of staged injection from struts. Gerlinger and Bruggemann⁷ conducted a numerical investigation of hydrogen injection from strut to foresee the

effects of lip thickness of the injector in mixing. They concluded that increase in lip thickness caused an increase in mixing layer due to the enhanced diffusivity associated with it and did not have much effect on mixing efficiency. Total pressure loss in the combustor was less affected by the height of the strut.

Computational fluid dynamics (CFDs) has proven to be an invaluable tool for the design and analysis of high-speed propulsion devices. Massive parallel computing, together with the maturation of robust CFD codes, has made it possible to perform simulations of complete engine flow paths. Navier-Stokes simulations are now widely used in the determination of optimum fuel injection configurations. The supersonic-reacting flow field can be described by adding finite rate chemistry to the standard compressible Navier-Stokes equation. The present solver used an RNG-based κ - ϵ two-equation turbulence model. The explicit treatment of all conservation terms result in stiffness and it degrades the performance of numerical method, as phenomena of differing time scales are solved simultaneously. Existence of several nonequilibrium states have created more difficulty in solution procedure. Bussing and Murman⁸ have introduced the method of preconditioning the conservation equations and treatment of chemical source terms alone implicitly and remaining explicitly, and found to have the advantage of both explicit and implicit methods. The developed solver is based on the two-dimensional Navier-Stokes equation governing compressible turbulent flows. The time integration is done using three-stage Runge-Kutta method. For modelling hydrogen-air reaction, an eight-step reaction mechanism proposed by Evans and Schexnayder⁹, has been used. Computations utilise laminar finite rate reaction kinetics.

Comparison of the numerical result has been carried out with the standard-reacting hydrogen wall jet experimental measurements of Burrows and Kurkov¹⁰. The predicted heat release and species production rates are in agreement with the experimental results. The analysis has been extended to study the mixing and reacting behaviour of planar hydrogen injection issuing into the hot supersonic airstream from diamond and wedge-shaped struts.

2. GOVERNING EQUATIONS

The equations, which govern a two-dimensional turbulent compressible flow in conservation form can be expressed in a generic form as

$$\frac{\partial U}{\partial t} + \frac{\partial(F - F_v)}{\partial x} + \frac{\partial(G - G_v)}{\partial y} = S \quad (1)$$

where

$$U = \begin{bmatrix} \rho \\ \rho u \\ \rho v \\ \rho E \\ \rho k \\ \rho \varepsilon \\ \rho Y_i \end{bmatrix}, F = \begin{bmatrix} \rho u \\ \rho u^2 + P \\ \rho uv \\ (\rho E + P)u \\ \rho uk \\ \rho u \varepsilon \\ \rho u Y_i \end{bmatrix}, G = \begin{bmatrix} \rho v \\ \rho vu \\ \rho v^2 + P \\ (\rho E + P)v \\ \rho vk \\ \rho v \varepsilon \\ \rho v Y_i \end{bmatrix}$$

$$F_v = \begin{bmatrix} 0 \\ \tau_{xx} \\ \tau_{xy} \\ Q_x \\ \mu_\kappa \frac{\partial u}{\partial x} \\ \mu_\varepsilon \frac{\partial \varepsilon}{\partial x} \\ D' \frac{\partial Y_i}{\partial x} \end{bmatrix} \text{ and } G_v = \begin{bmatrix} 0 \\ \tau_{xy} \\ \tau_{yy} \\ Q_y \\ \mu_\kappa \frac{\partial v}{\partial y} \\ \mu_\varepsilon \frac{\partial \varepsilon}{\partial y} \\ D' \frac{\partial Y_i}{\partial y} \end{bmatrix}$$

$$\text{Source vector } (S) = [0 \quad 0 \quad 0 \quad H_k \quad H_\varepsilon \quad \omega]^T$$

$$Q_x = u\tau_{xx} + v\tau_{xy} + k_{eff} \frac{\partial T}{\partial x} \text{ and}$$

$$Q_y = u\tau_{xy} + v\tau_{yy} + k_{eff} \frac{\partial T}{\partial y}$$

The effective exchange coefficient for the diffusion process can be calculated as

$$D' = \frac{\mu_t}{Sc_t} + \frac{\mu_l}{Sc_l}$$

$$k_{eff} = k_l + k_t$$

$$\text{in which, } k_t = \frac{\mu_l C_p}{Pr}, k_l = \frac{\mu_l C_p}{Pr_l} \text{ and } \mu_{eff} = \mu_l + \mu_t$$

From Sutherland's law, laminar viscosity becomes:

$$\mu_l = 1.458 \times 10^{-6} \frac{T^{1.5}}{T + 110.4}$$

and μ_t can be calculated from the turbulence model.

For the present analysis, a modified κ - ε model called renormalisation group (RNG) model was used. Yakhot¹¹, *et al.* proposed this model, which systematically removes all the small scales of turbulence motion from the governing equation by expressing their effects in terms of large scales and a modified viscosity.

$$\frac{\partial(\rho\kappa)}{\partial t} + \text{div}(\rho\kappa U) = \text{div}[\alpha_\kappa \mu_{eff} \text{grad}\kappa] + H_\kappa \quad (2)$$

$$\frac{\partial(\rho\varepsilon)}{\partial t} + \text{div}(\rho\varepsilon U) = \text{div}[\alpha_\varepsilon \mu_{eff} \text{grad}\varepsilon] + H_\varepsilon \quad (3)$$

Here the turbulence source terms are obtained as

$$H_\kappa = 2\mu_t E_{ij} - \rho\varepsilon \text{ and}$$

$$H_\varepsilon = C_{1\varepsilon}^* \frac{\varepsilon}{\kappa} 2\mu_t E_{ij} \cdot E_{ij} - C_{2\varepsilon} \rho \frac{\varepsilon^2}{\kappa}$$

The turbulent viscosity is defined as

$$\mu_t = \rho C_\mu \frac{k^2}{\varepsilon}$$

The closure coefficients are:

$$C_\mu = 0.08, \alpha_\kappa = \alpha_\varepsilon = 1.39, C_{1\varepsilon} = 1.42, C_{2\varepsilon} = 1.68$$

$$\eta = \sqrt{(2E_{ij} \cdot E_{ij})^{\kappa/\varepsilon}}, C_{1\varepsilon}^* = C_{1\varepsilon} - \frac{\eta(1 - \eta/\eta_0)}{1 + \beta\eta^3} \text{ and}$$

$$\eta_0 = 4.37, \beta = 0.01$$

The value of constant β is adjustable which can be calculated from the near-wall turbulence data. All the other parameters are explicitly computed as a part of the RNG calculations.

For modelling hydrogen-air reaction, an eight-step reaction mechanism⁹ has been used for which the reaction steps and reaction rates are presented in Table 1.

From the law of mass action applicable for any chemical reaction, one has:

$$\sum_{i=1}^N \gamma'_{ji} C_i \longleftrightarrow \sum_{i=1}^N \gamma''_{ji} C_i$$

$$(\dot{C}_i)_j = (\gamma''_{ji} - \gamma'_{ji}) \left[k_{f_j} \prod_{i=1}^N C_i^{\gamma'_{ji}} - k_{b_j} \prod_{i=1}^N C_i^{\gamma''_{ji}} \right] \quad (4)$$

where $i = 1, 2, 3, \dots$ represents species and $j = 1, 2, 3, \dots$ represents reactions.

Net change in concentration of any species can be found as

$$\dot{C}_i = \sum_{j=1}^{N_R} (\dot{C}_i)_j \quad (5)$$

and the net production of species is given by

$$\dot{\omega}_i = \dot{C}_i W_i \quad (6)$$

The forward and backward reaction rates in the above equation are the functions of temperature, that can be calculated from the Arrhenius law, using coefficients presented in Table 1. The evaluation of thermodynamic properties such as specific heat at constant pressure, and enthalpy can be calculated from the standard thermodynamic data (McBride and Gordon¹²) as

$$\frac{C_{p_i}}{R} = A_i + B_i T + C_i T^2 + D_i T^3 + E_i T^4 \quad (7)$$

$$\frac{H_i}{RT} = A_i + \frac{B_i}{2} T + \frac{C_i}{3} T^2 + \frac{D_i}{4} T^3 + \frac{E_i}{5} T^4 + \frac{F_i}{T} \quad (8)$$

For each species two sets of coefficients are used for the temperature intervals, one applicable from 300K up to 1000K and the other applicable from 1000K up to 3000K. Total energy of flow field is given by

$$E = \sum_{i=1}^{N_i} Y_i h_i - \frac{p}{\rho} + \frac{1}{2} (u^2 + v^2) \quad (9)$$

Temperature is worked out from the above equation using the Newton-Raphson method. The pressure is calculated from the resulting temperature as follows:

$$p = \rho R \sum_{i=1}^{N_i} \frac{Y_i}{W_i} T \quad (10)$$

Table 1. Reaction steps and reaction rates

Reaction	Forward reaction rates			Backward reaction rates		
	A	n	E	A	n	E
$H_2+M = H+H+M$	5.5×10^{18}	-1.0	51987.0	1.8×10^{18}	-1.0	0
$O_2+M = O+O+M$	7.2×10^{18}	-1.0	59340.0	4.0×10^{17}	-1.0	0
$H_2O+M = H+OH+M$	5.2×10^{21}	-1.5	59386.0	4.4×10^{20}	-1.5	0
$OH+M = O+H+M$	8.5×10^{18}	-1.0	50830.0	7.1×10^{18}	-1.0	0
$H_2O+O = OH+OH$	5.8×10^{13}	0.0	9059.0	5.3×10^{12}	0.0	503
$H_2O+H = OH+H_2$	8.4×10^{13}	0.0	10116.0	2.0×10^{13}	0.0	2600
$O_2+H = OH+O$	2.2×10^{14}	0.0	8455.0	1.5×10^{13}	0.0	0
$H_2+O = OH+H$	7.5×10^{13}	0.0	5586.0	3.0×10^{13}	0.0	4429

Reaction rates are expressed in the Arrhenius law form, $k = AT^N \exp\left(-\frac{E}{RT}\right)$ and M is the third body.

3. NUMERICAL METHOD

Basically, finite volume technique is an integration of conservation laws. In other words, mass, momentum and energy should be conserved at the basic discrete level. The conservation equation applicable for a cell is:

$$\frac{\partial U}{\partial t} + \nabla \cdot F - S = 0 \quad (11)$$

Distributing the integral and applying Greens theorem, one has:

$$\int_{\Omega} \frac{\partial U}{\partial t} d\Omega + \int_{\Gamma} F n d\Gamma - \int_{\Omega} S d\Omega = 0 \quad (12)$$

where Γ is the total surface area and Ω is the cell volume.

$$\frac{dU_i}{dt} V_i + \sum_{faces} F \cdot ds - S_i \cdot V_i = 0 \quad (13)$$

where V_i is the cell volume and ds is the area of elemental sides.

This is a system of ordinary differential equation. For obtaining the solution, this equation has to be integrated wrt time. The cell averages of the derivative of different flow variables for the surface described by a quadrilateral ABCD can be evaluated as

$$\left(\frac{\partial U}{\partial x} \right)_{ABCD} = \frac{(U_A - U_C)(y_B - y_D) - (U_B - U_D)(y_A - y_C)}{(x_A - x_C)(y_B - y_D) - (x_B - x_D)(y_A - y_C)}$$

$$\left(\frac{\partial U}{\partial y} \right)_{ABCD} = \frac{(x_A - x_C)(U_B - U_D) - (x_B - x_D)(U_A - U_C)}{(x_A - x_C)(y_B - y_D) - (x_B - x_D)(y_A - y_C)}$$

For the simple explicit scheme, the time stepping using Runge Kutta method can be described as

$$U_i^{(0)} = U_i^{(n)}$$

$$U_i^{(1)} = U_i^{(0)} - \alpha_1 \frac{\Delta t_i}{V_i} (R_i^{(0)} - D_i^{(0)})$$

$$U_i^{(2)} = U_i^{(0)} - \alpha_2 \frac{\Delta t_i}{V_i} (R_i^{(1)} - D_i^{(0)})$$

$$U_i^{(3)} = U_i^{(0)} - \alpha_3 \frac{\Delta t_i}{V_i} (R_i^{(2)} - D_i^{(0)})$$

$$U_i^{n+1} = U_i^n + U_i^{(3)} \quad (15)$$

$$\alpha_1 = 0.6, \alpha_2 = 0.6 \text{ and } \alpha_3 = 1.0$$

Governing equations of turbulent shear layer flows, involving finite rate chemistry, are often difficult to solve due to their stiffness (ratio of largest time scale to smallest time scale). Stiffness degrades the performance of numerical methods. While handling two phenomena of differing time scales together, both can be advanced equally in pseudo time. In other words, it can be treated as way of rescaling⁸ the equation on time such that both phenomena evolve at comparable pseudo time scales. Then, the fast process will not hold the slower process. Thereby, higher time steps can be achieved. Thus the modified equation is:

$$SJ \frac{\partial U}{\partial t} + \frac{\partial F}{\partial x} + \frac{\partial G}{\partial y} = S \quad (16)$$

The point implicit formulation of the time stepping can be written as

$$\overline{U_i^{(0)}} = \overline{U_i^{(n)}}$$

$$\overline{SJ^0} \left(\overline{U_i^{(1)}} - \overline{U_i^{(0)}} \right) = -\alpha_1 \frac{\Delta t_i}{V_i} \left(\overline{R_i^{(0)}} - \overline{D_i^{(0)}} \right)$$

$$\overline{SJ^1} \left(\overline{U_i^{(2)}} - \overline{U_i^{(0)}} \right) = -\alpha_2 \frac{\Delta t_i}{V_i} \left(\overline{R_i^{(1)}} - \overline{D_i^{(0)}} \right)$$

$$\overline{SJ^3} \left(\overline{U_i^{(3)}} - \overline{U_i^{(0)}} \right) = -\alpha_3 \frac{\Delta t_i}{V_i} \left(\overline{R_i^{(3)}} - \overline{D_i^{(0)}} \right) \quad (17)$$

$$\overline{U_i^{n+1}} = \overline{U_i^n} + \overline{U_i^{(3)}}$$

$$\alpha_1 = 0.6, \alpha_2 = 0.6 \text{ and } \alpha_3 = 1.0$$

In the point implicit scheme, all the six chemical species (H_2 , O_2 , OH , H , O and H_2O) are treated implicitly, while all the other species are treated explicitly. The preconditioning matrix SJ used for this purpose is given by

$$SJ = \begin{bmatrix} 1 - \alpha_i \Delta t \frac{\partial \omega_{H_2}}{\partial Y_{H_2}} & -\alpha_i \Delta t \frac{\partial \omega_{H_2}}{\partial Y_{O_2}} & \dots & -\alpha_i \Delta t \frac{\partial \omega_{H_2}}{\partial Y_{H_2O}} \\ -\alpha_i \Delta t \frac{\partial \omega_{O_2}}{\partial Y_{H_2}} & 1 - \alpha_i \Delta t \frac{\partial \omega_{O_2}}{\partial Y_{O_2}} & \dots & -\alpha_i \Delta t \frac{\partial \omega_{O_2}}{\partial Y_{H_2O}} \\ \dots & \dots & \dots & \dots \\ -\alpha_i \Delta t \frac{\partial \omega_{H_2O}}{\partial Y_{H_2}} & -\alpha_i \Delta t \frac{\partial \omega_{H_2O}}{\partial Y_{O_2}} & \dots & 1 - \alpha_i \Delta t \frac{\partial \omega_{H_2O}}{\partial Y_{H_2O}} \end{bmatrix} \quad (18)$$

4. RESULTS AND DISCUSSION

4.1 Hydrogen Wall-attached Jet Issuing to Hot-vitiated Airstream

The prediction capability of the code for chemical reaction in a supersonic flow field was analysed using a validation test data obtained from the Burrows and Kurkov experiment¹⁰. A sonic stream of hydrogen was injected to hot-vitiated airstream along a slightly angled down wall. The schematic of the setup is shown in Fig.1. The flow field conditions are summarised in Table 2. The left face of the computational domain is given with a supersonic inflow condition in the region of supersonic airstream. Hydrogen jet with the abovementioned conditions was introduced at the respective position as separate boundary condition. The bottom wall is a no-slip wall and the top face is a free-slip wall so that the coarse grid could be applied in this region (to save

computational resources). All the flow features are confined to near-bottom wall. A supersonic outflow condition is maintained at the outlet. For capturing high gradients near to the bottom-angled wall (due to wall boundary layer and mixing layer between hydrogen and airstream), a fine grid of uniform size (0.1 mm in y-direction) was provided up to 1.5 cm above the wall. Peak temperature showed (using this grid) slight deviation from the experimental value. To prove the grid independence of the results, the grid size in this region only was reduced to half of the previous trial. A total number of control volumes have become 74000. A comparison of temperature predictions is shown in Fig. 2. It followed the previous curve except at the centre of the shear layer, giving more close prediction for the peak value. A detailed comparison of the computed results (of two trials with the abovementioned grid sizes) with the experimental data for chemical species

Table 2. Test conditions in Burrows and Kurkov¹⁰ experiment

Free-stream conditions	H ₂ jet	Vitiated air stream
Mach number	1.0	2.44
Temperature (K)	254.0	1270.0
Pressure (Pa)	101325	101325
H ₂ mass fraction	1.0	0
H ₂ O mass fraction	0	0.256
O ₂ mass fraction	0	0.258
N ₂ mass fraction	0	0.486

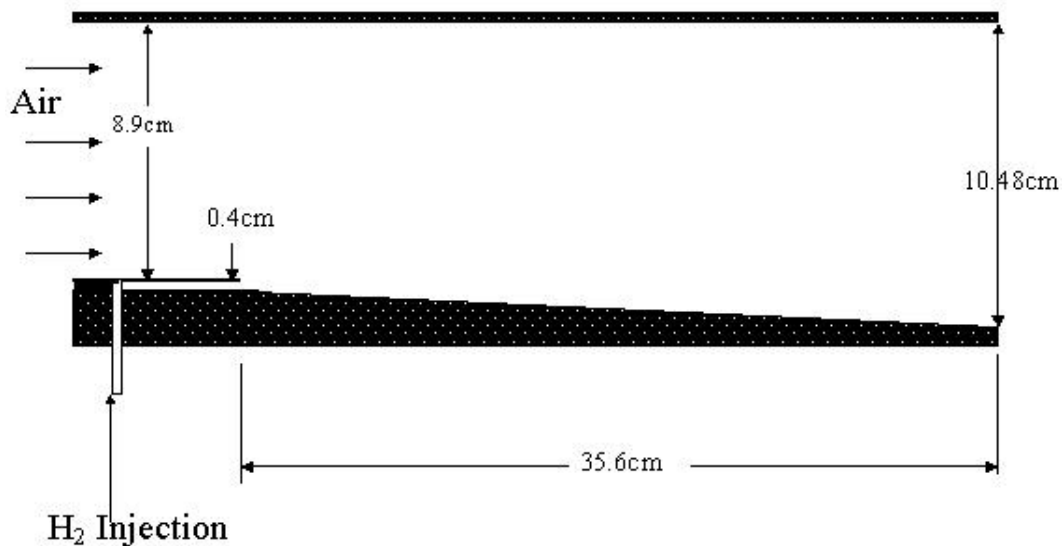


Figure 1. Experimental setup of Burrows and Kurkov¹⁰

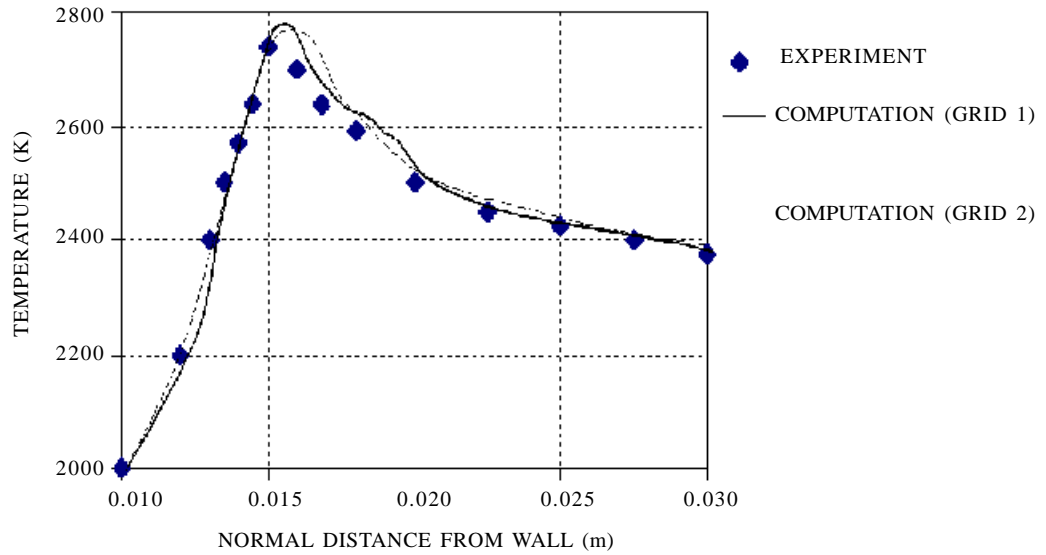


Figure 2. Comparison of predicted temperature in mixing layer at exit plane.

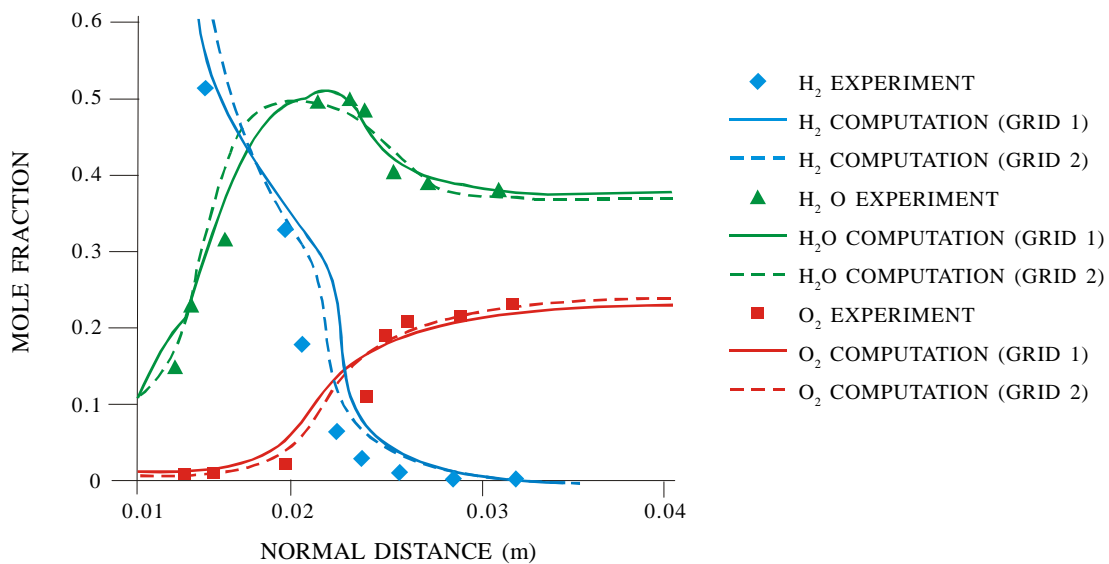


Figure 3. Comparison of computed results with experimental data for species mole fraction profiles at exit plane.

is shown in Fig. 3. The predicted variations of species mole fractions were in good agreement with the experimental data.

The introduction of point implicit technique was found to be effective in dealing with chemical source terms. The CFL (Courant, Friedrichs and Lewis) number almost equal to that of compressible turbulent flow (without reaction) could successfully demonstrate this phenomenon. The average non-reacting hydrogen concentration was found to be

decreasing along the wall and it caused a small decrease in temperature and did not overcome by increase in mixing and reaction. The flame spread upwards as it moved along the wall.

4.2 Parallel Injection Downstream of a Diamond-shaped Strut

In real scramjet combustor, the flow field is extremely complex. The parallel injection has the advantage of momentum addition and the pressure

loss is minimum. But the mixing efficiency of such systems is very low when compared to transverse injections. However, the mixing behaviour of the planar jet could be enhanced by the artificial production of recirculation zone due to shock wave-expansion wave pattern. Strut is capable of injecting the fuel directly to the core of the supersonic flow. Shock wave-aided mixing approach has been useful in parallel injection from struts. The objective of the present study is to depict the flow features of the supersonic turbulent-reacting flow field, resulting due to hydrogen injection from a strut to a supersonic airstream.

Schematic of the computational domain is given in Fig. 4. A sonic stream of hydrogen ($p = 1.60$ bar and $T = 500$ K) was injected parallel to a supersonic ($M = 2$) airstream hydrogen ($p = 0.72$ bar and $T = 1050$ K) through an injector of diameter 0.30 mm placed on an axial strut of height 6.00 mm and lip height 1.00 mm. The computational domain was discretised into 86000 control volumes, and the flow field was initialised with free-stream conditions. The top and bottom walls were given with no-slip wall condition and the minimum grid size in this region was 0.05 mm. The calculated pressure distribution

is shown in Fig. 5. The shock waves and expansion waves along and downstream of the strut is well-captured. The Schlieren images from the experiments of Gerlinger and Bruggemann⁷ revealed the presence of similar wave pattern. When the hydrogen stream was injected through the core of such flow field, localised recirculation regions created downstream of the jet, which enhanced the mixing. Vector plot of the region immediate to jet outlet is shown in Fig. 6. It revealed the presence of vortices near the lip. The enlarged field view of the variations of Mach number in the flow field near to the injector exit is shown in Fig. 7. Low-velocity regions could be identified along the path of progress of the hydrogen jet. Alternate compression and expansion took place for the jet and was not enough to perturb the flow field much in the region near to the jet outlets. But the shock wave/expansion wave reflections interfered with the upcoming jet and localised low-velocity regions, were produced. Though, these regions are responsible for pressure loss of the jet, certainly enhanced the mixing and reaction. Lip height plays an important role in mixing enhancement. Water mass fraction plot for the flow field downstream of the injector is shown in the Fig. 8. The water

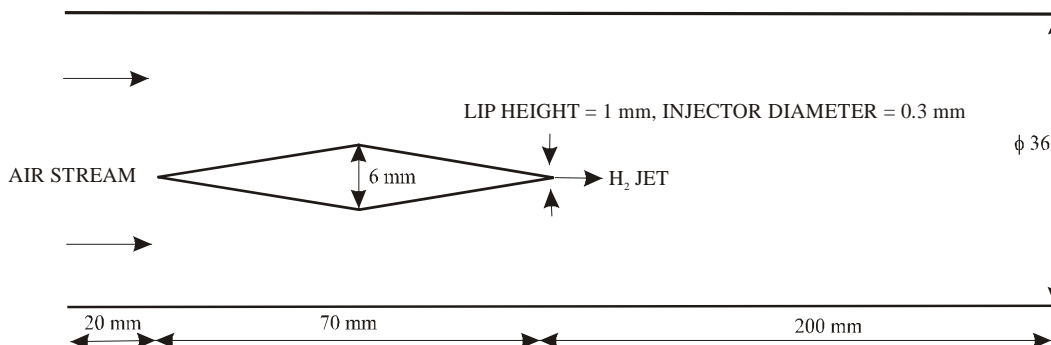


Figure 4. Schematic of the computational domain for a strut injector.

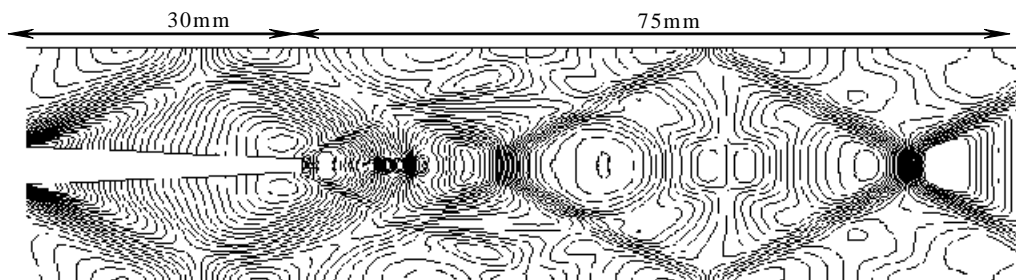


Figure 5. Pressure contours downstream of the strut.

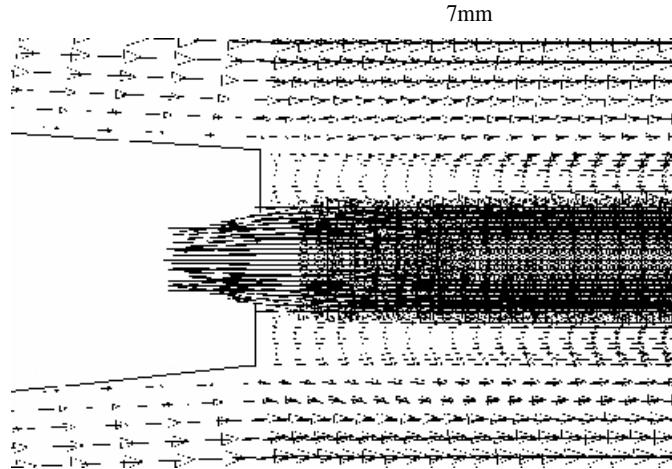


Figure 6. Vector plot of the region immediate to jet outlet.

concentration is found to be more in the shear layer formed between the two streams of flow and the low-velocity recirculation regions within the core of the upcoming jet. Since the penetration of the jet is low, water species production is confined to aforesaid areas only. The temperature of the resulting flow and reaction is shown in Fig. 9. It is found that the maximum temperature occurred in the recirculation areas, produced due to shock wave/expansion wave-jet interaction and fuel jet losses concentration, the temperature decreased slightly along the axis. Figure 10 gives the field view of the *OH* species mass fraction. The order of magnitude of *OH* species production was much low compared to that of water, as its conversion occurred at a faster rate.

4.3 Combustion of Hydrogen in the Wake Region of Strut

The numerical simulation of the flow field generated by the injection of a sonic stream of hydrogen jet into the hot airstream has been performed. The geometry used for the present analysis is similar to that proposed by Welper and Koschel^{13,14} and is shown in Fig. 11. The wake region formed due to the wedge-shaped strut enhanced the mixing of the upcoming hydrogen jet. In addition to this reflected oblique shocks and its reflections from upper and lower walls along with the expansion wave from the lip of the strut interacted with this wake region and the jet in its core. This led to the formation of localised low-velocity regions blocking the progress

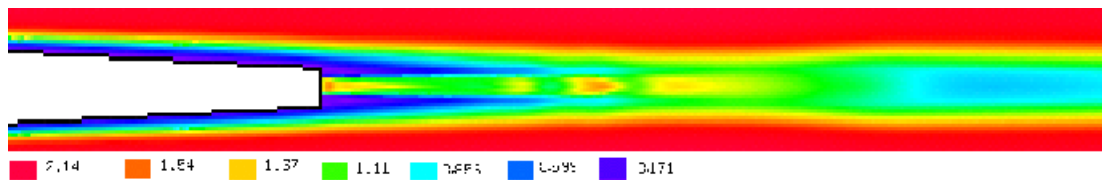


Figure 7. An enlarged Mach number field view of the region near to jet.

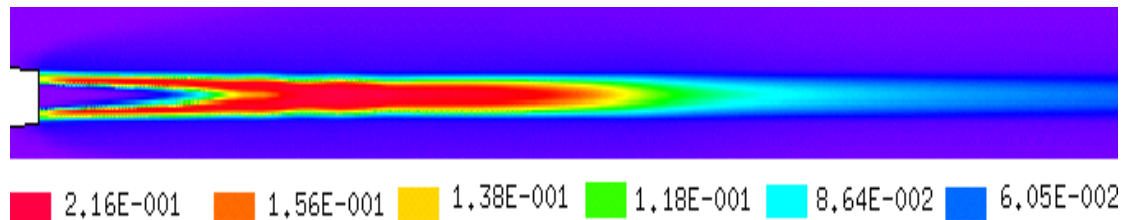


Figure 8. Field view of water mass fraction for the region downstream of the strut.

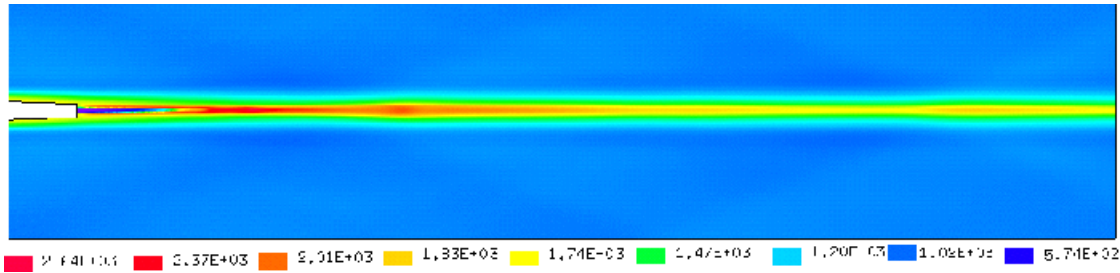


Figure 9. Field view of temperature for the region down stream of the strut.

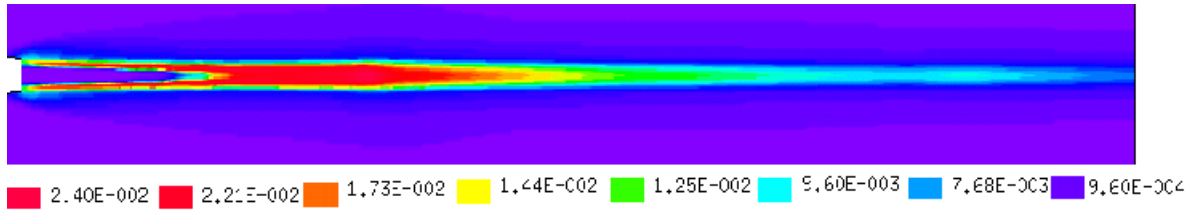


Figure 10. Field view of OH mass fraction for the region down stream of the strut.

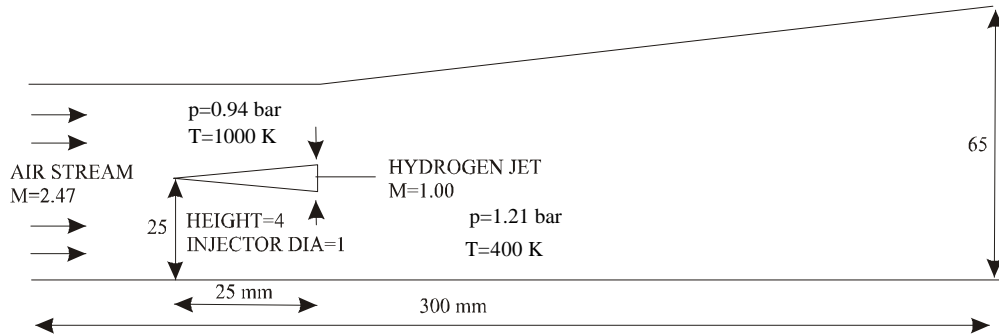


Figure 11. Schematic of the computational domain for strut injection.

of the jet and hence sustained reaction zones in its outer periphery. But on the other hand, the same phenomenon led to the pressure loss, which decides the total available thrust at the nozzle exit of the engine.

For the present analysis, the geometry was divided into 105600 control volumes. The flow conditions for free-stream and hydrogen injection are summarised in Table 3. Here the top and bottom walls were given with no-slip walls condition and minimum grid size in this region was maintained at 0.01 mm.

The converged results are post-processed and the field view of Mach number is shown in Fig. 12. The oblique shock and its successive reflections are well-captured. The alternate compression and expansion of the over-expanded hydrogen jet and

its interaction with shock reflection could be observed. Due to the effect of wake, localised recirculation zones with high residence time are created. Sustained combustion and high temperature occurred in these areas that could be observed from the field view of temperature (Fig. 13). The oblique shock originated from the leading edge of the strut created an increase in temperature. This along with low-velocity region in the lip initiated the combustion. Further downstream the localised reaction pools generated due to shock wave and expansion wave interaction with wake-jet core system enhanced the mixing and the reaction. Along the length of the combustor, the flame is found to be laterally spreading as the eddy systems grew in size. Water mole fraction plot shown in Fig. 14 also revealed the mixing enhancement and reaction in wake-jet interaction region.

Table 3. Test condition in strut injection computational

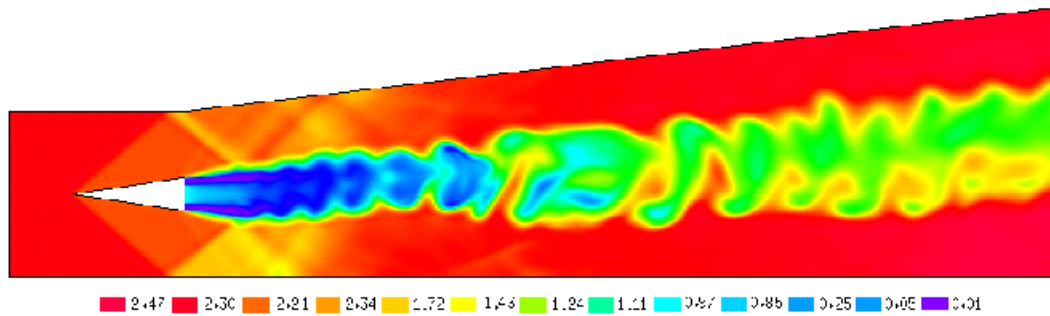
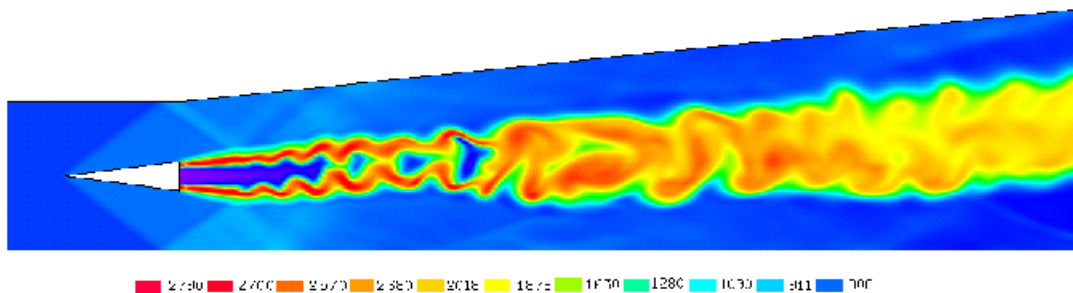
Free stream conditions	H ₂ jet	Air stream
Mach number	1.0	2.47
Temperature (K)	400.0	800
Pressure (Pa)	121000	94000
H ₂ mass fraction	1.0	0
H ₂ O mass fraction	0	0
O ₂ mass fraction	0	0.23
N ₂ mass fraction	0	0.77

Oevermann¹⁵ analysed a similar scramjet combustor geometry with a stretched laminar flamelet model for turbulent diffusion flames in which coupling between turbulence and nonequilibrium chemistry is achieved via statistical description of the mixture fraction with a presumed probability density function (PDF) and a mean turbulent strain rate acting on the flame. In this study, grid is adapted in the vicinity of shock wave expansion wave reflections to capture its effects completely. The present study could not capture the complete wave reflections due to the enhanced numerical dissipation effects of the numerical scheme and lack of grid clustering near-downstream shock reflections.

5. CONCLUSIONS

Computational analysis of supersonic turbulent-reacting flow field has been performed with point implicit finite volume method on unstructured grids. The preconditioning used for chemical source terms has been found to improve the capability of the code by increasing the CFL to 0.5 mm, almost equal to that of the non-reacting version of the same code. A comparison of the computed data with the experimental data has shown reasonable agreement.

The computational analysis of parallel injection from diamond-shaped strut could reveal the flow structure of progress of hydrogen jet through the areas disturbed by the reflections of oblique shock. The recirculations in the lip area of the orifice and the shock reflections are well-captured. It is found that the maximum temperature occurred in the recirculation areas (produced due to shock wave-expansion wave-jet interaction and the fuel jet losses concentration) after passing successively through such areas, temperature decreased slightly along the axis.

**Figure 12. Mach number field view of combustion zone.****Figure 13. Field view of temperature.**

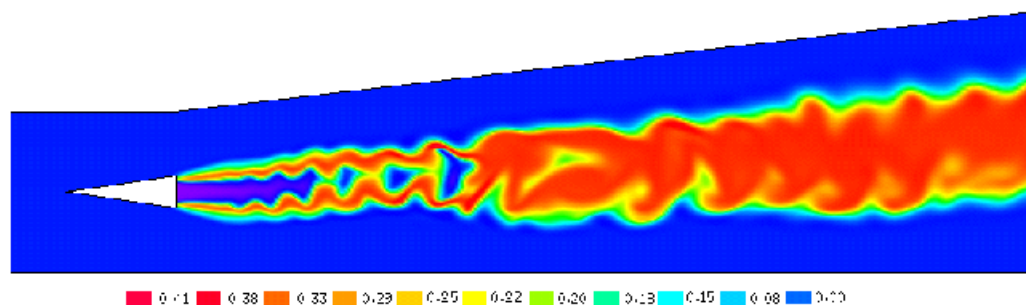


Figure 14. Field view of water mass fraction.

The complex flow field generated from the injection of hydrogen from wedge-shaped strut is revealed in the analysis. It is found that the localised reaction pools generated due to shock/wave and expansion wave interaction with wake-jet core system enhanced the mixing and the reaction. Water mole fraction is found to be high in the wake-jet interaction region due to the mixing enhancement and high residence time. Though the eight-step chemical kinetic mechanism employed here is performing well when coupled with two-dimensional turbulent compressible Navier-Stokes equation; difficulties were experienced in computational procedure due to more number of variables.

ACKNOWLEDGEMENTS

Mr M. Deepu is thankful to Dr T. Jayachandran, Head of Fluid Mechanics and Thermal Analysis Division of Propulsion Group, Vikram Sarabhai Space Centre, Thiruvananthapuram and his team members for their valuable suggestions for this work.

REFERENCES

1. Gruber, M.R. & Nejad, A.S. New supersonic combustion research facility. *J. Prop. Power*, 1995, **11**(5), 1080-83.
2. Riggins, D.W. & McClinton, C.R. A computational investigation of flow losses in a supersonic combustor. AIAA Paper No. 90-2093, 1990.
3. Riggins, D.W.; McClinton, C.R. & Vitt, P.H. Thrust losses in hypersonic engines—Part 1: Methodology. *J. Prop. Power*, 1997, **13**(2).
4. Riggins, D.W.; McClinton, C.R. & Vitt, P.H., Thrust losses in hypersonic engines—Part 2: Applications. *J. Prop. Power*, 1997, **13**(2).
5. Tomioka, S.; Kanda, T.; Tani, K.; Mitani, T.; Shimura, T. & Chinzei, N. Testing of a scramjet engine with a strut in M8 flight conditions. AIAA Paper No. 98-3134, 1998.
6. Tomioka, S. Combustion tests of a staged supersonic combustor with a strut. AIAA Paper No. 98-3273, 1998.
7. Gerlinger, P. & Bruggemann, D. Numerical investigation of hydrogen strut injections into supersonic air flows. *J. Prop. Power*, 2000, **16**(1), 22-28.
8. Bussing, T.R.A. & Murman, E.M. Finite volume method for the calculation of compressible chemically reacting flows. *AIAA Journal*, 1988, **26**(4), 1070-78.
9. Evans, J.S. & Schexnayder, C.J. Influence of chemical kinetics and unmixedness on burning supersonic hydrogen flames. *AIAA Journal*, 1980, **18**(1), 188-93.
10. Burrows, M.C. & Kurkov A.P. Analytical and experimental study of supersonic combustion of hydrogen in a vitiated airstream. NASA, Washington, D.C., 1973. NASA TM X-2828.
11. Yakhot, V.; Orzag, A.; Gatski, T.B. & Speziade, C.B. Development of turbulence model for shear flows by a double expansion technique. *Physics of Fluids*, 1992, **4**, 1510-520.
12. McBride, B.J. & Gordon, S. Computer program for calculation of complex chemical equilibrium compositions, rocket performance, incident and reflected shocks, and Chapman-Jouget detonations. NASA, Washington, D.C., 1971. NASA SP-273.

13. Welper, U. & Koschel, W. Numerical investigations of turbulent-reacting flows in a scramjet combustor model. AIAA Paper No. 2002-3572, 2002.
14. Welper, U. & Koschel, W. Numerical investigations of shock wave/mixing layer interaction in a scramjet combustion chamber. International Symposium on Computational Fluid Dynamics, 1999, Bremen, Germany.
15. Oevermann, M. Numerical investigation of turbulent hydrogen combustion in a scramjet using flamelet modelling. *Aero. Sci. Technol.*, 2000, **4**, 463-80.

Contributors



Mr M. Deepu obtained his MTech (Thermal Sciences) from the University of Kerala in 2001. Presently, he is working as Senior Lecturer in Mechanical Engineering Department of N.S.S. College of Engineering, Palakkad. His areas of research include computational fluid dynamics (CFD), reacting flows, and heat transfer. He has published 15 papers in national and international journals and conferences.



Dr S.S. Gokhale obtained his PhD from the University of Illinois at Champaign-Urbana, USA. After serving in the Department of Aerospace Engineering at IIT Madras, Chennai, for nearly 23 years, currently he is the Director of VNIT, Nagpur. His areas of research are CFD, multiphase flows, simulation, and optimisation. He has published 30 papers in the national and international journals and conferences.



Dr S. Jayaraj obtained his PhD (Engg) from IIT, Kanpur, in 1988. He joined as Lecturer at the REC, Calicut, in 1981. Presently, he is working as Professor at the National Institute of Technology, Calicut. He has guided three students for PhD and more than 30 for MTech. He has published 12 papers in international journals and more than 25 in international conferences. His areas of research include microchannels, CFD, heat transfer, refrigeration and airconditioning, and energy conservation and management.